NEW INFRARED OBJECTS ASSOCIATED WITH OH MASERS

N. J. EVANS II*†

Owens Valley Radio Observatory, California Institute of Technology, and
Department of Astronomy and McDonald Observatory, University of Texas at Austin

AND

S. BECKWITH

Department of Physics, California Institute of Technology

ABSTRACT

Infrared sources have been found at 10μm near the position of six OH masers which were previously unidentified with any optical or 2μm object. The OH masers selected for the search have good radio positions and emit principally at 1612 MHz in two distinct velocity ranges. All the sources have varied in time, and significant variations in color temperature have been detected in two objects. The 2 to 20μm energy distributions of the sources are extremely red, and four of the objects show silicate absorption features, in striking contrast to previously studied infrared sources associated with such OH masers.

Measured OH and infrared fluxes are consistent with pumping of the OH maser by 35μm photons, but argue strongly against pumping at 2.8μm. The observations are consistent with a model for these objects as distant (2–10 kpc), luminous ($L \approx 10^4 L_\odot$) stars with very thick circumstellar dust shells at temperatures around 500 K. Two of the objects display absorption in the 2.3μm band of CO, linking them to previously studied OH/IR objects which are Mira variables or M supergiants. The other four objects have some characteristics which are different from previously studied OH/IR objects; the thick dust shells indicated in these four objects suggest a further evolution, perhaps leading to planetary nebula formation.

Subject headings: infrared: sources — masers — stars: circumstellar shells — stars: long-period variables

I. INTRODUCTION

Following the discovery of OH maser emission from extremely red stellar objects (Wilson and Barrett 1968), several searches were made for OH emission from objects in the 2.2μm sky survey (Neugebauer and Leighton 1969). Objects were selected on the basis of their redness and, by virtue of the detection limit of the 2.2μm survey, their strength at 2.2μm. The 20 OH masers found in this way are all oxygen-rich M-type Mira variables or M supergiants (Hyland *et al.* 1972). The strong emission at $\lambda > 3 \mu$m was interpreted as thermal radiation from dust in a circumstellar envelope. Although the statistics are poor, the fraction of 2.2μm sources which show OH emission appears to increase with redness, indicating a correlation between dust shell thickness and the probability of an OH maser. In fact, if carbon stars are excluded, the fraction of the very reddest Mira variables associated with OH masers becomes 50%–100% (Hyland *et al.* 1972). Harvey *et al.* (1974) studied the infrared and radio variation of 14 masers and noted a strong correlation, indicating an infrared pumping mechanism for the OH emission.

The OH maser emission from infrared stars is

characteristically strongest at 1612 MHz and confined to two distinct velocity ranges. As a result, the terminology "OH/IR" or "Type IIb OH/IR" has often been used for such masers, even before an infrared star has been found (e.g., Winnberg *et al.* 1973). In fact, there is a large and growing list of 1612 MHz OH masers with double-peaked velocity structure which have neither optical identifications nor associated objects in the 2.2μm sky survey (Caswell 1974). These "unidentified" masers were discovered either by accident or by surveys, generally of strips along the galactic plane (e.g., Winnberg *et al.* 1973).

In order to determine whether these unidentified maser sources are actually associated with infrared sources, we have searched for infrared radiation at 10μm from a sample of the OH sources. The OH sources used in the sample were found in a survey of four strips along the galactic plane that resulted in the discovery of 13 OH sources (Winnberg *et al.* 1973; Andersson *et al.* 1974). Positions with $\sim 5''$ accuracy were measured for nine of these sources (Evans, Crutcher, and Wilson 1976). Of these nine, six show the double-peaked velocity structure. These six OH sources form the sample for the present study.

II. OBSERVATIONS

The sources observed are listed in Table 1. The observations covered the period 1974 July to 1976 May.

729

TABLE 1
INFRARED AND RADIO POSITIONS OF NEW SOURCES

Source (1)	Type (2)	R.A. (1950) (3)	Decl. (1950) (4)
OH 21.5+0.5....	Radio	$10^h25^m44^s1$	$-10°00'08''$
	Infrared	10 25 45.5	-10 00 14
OH 26.5+0.6....	Radio	18 34 52.2	-05 26 34
	Infrared	18 34 52.6	-05 26 37
OH 30.1−0.2....	Radio	18 44 32.7	-02 38 57
	Infrared	18 44 33.0	-02 38 56
OH 30.1−0.7....	Radio	18 46 04.4	-02 53 55
	Infrared	18 46 05.0	-02 53 57
OH 32.8−0.3....	Radio	18 49 47.7	-00 17 48
	Infrared	18 49 48.0	-00 17 55
OH 45.5+0.1....	Radio	19 11 58.3	$+11$ 05 25
	Infrared	19 11 58.3	$+11$ 05 20

Dates of specific measurements are given in Table 2. The infrared search was made at a wavelength of 10 μm by using the 1.5 m telescope at Mount Wilson and the photometric system described by Beckwith et al. (1976). An area around the OH position was scanned until a source was found. The positions of the infrared sources, shown in Table 1, were established relative to nearby field stars, whose positions were then determined by measurement of the Palomar Sky Survey plate. The positions obtained in this way are accurate to $\pm 4''$. Photometric measurements of the sources from 2 to 20 μm were made with a 9″ aperture; those made before 1976 were made with the wavelength bands listed by Beckwith et al. (1976). Slightly different filters were used for the 1976 measurements; the effect of this change is discussed later. In most cases, observations were made on two separate nights at each listed time to check consistency. Observations of the 2.3 μm vibration band of CO were made for three of the sources. The remaining three sources were not observed because of their extreme faintness at 2 μm. Initial observations were obtained at the 1.5 m telescope by using the filter wheel spectrometer described by Neugebauer et al. (1976). The resolution was 1.2% $(\Delta\lambda/\lambda)$, and measurements were made at intervals of 0.039 μm. The spatial aperture was 7″5; sky subtraction was accomplished by chopping 14″ in declination. Subsequently, similar observations were made on the 2.1 m telescope at the Kitt Peak National Observatory. The filter wheel at KPNO has a resolution of 1.4% $(\Delta\lambda/\lambda)$, and data were taken at intervals of 0.014 μm.

Observations of the OH emission at 1612 MHz were made with the 40 m antenna at Owens Valley in 1975 December and June with a beam size of 20″2. A 100-channel autocorrelator was used with a velocity resolution of 0.47 km s^{-1}. The signals were calibrated versus a noise tube, and a flux density scale was established by observation of known continuum sources.

Observations of the $J = 1 \rightarrow 0$ transition of ^{12}CO were made at the 5 m antenna of the Millimeter Wave Observatory.[1] The beam size was 2″3, the velocity resolution was 5.2 km s^{-1}, and the velocity coverage

was ~100 km s^{-1}. Calibration was accomplished by means of a rotating chopper wheel. Observations of the $J = 1 \rightarrow 0$ transition of ^{13}CO were also made at the 11 m antenna of the National Radio Astronomy Observatory,[2] at Kitt Peak. The beam size was 1″2. Two filter banks were used in parallel. One covered a velocity range of 70 km s^{-1} at a resolution of 0.27 km s^{-1}, while the other covered a velocity range of 174 km s^{-1} at a resolution of 0.68 km s^{-1}. A chopper wheel was used for calibration and was supplemented by periodic observations of sources with known ^{13}CO emission strengths. The results are shown in Table 5.

III. RESULTS

a) Positions and Identifications

An infrared source was discovered at 10 μm near the position of each of the six OH sources in the sample. In five cases, the positions of the infrared sources, presented in Table 1, agree within the uncertainties with the OH positions reported by Evans, Crutcher, and Wilson (1976). The infrared and OH positions of OH 21.5+0.5 differ by 21″ in right ascension. No infrared source could be found in a 15″ × 15″ box around the nominal OH position stronger than 0.5 Jy (3 σ). Evans (1976) reports that there is a possible systematic error in right ascension in their data.

The infrared emission of each of the sources has varied since its discovery. For all of the sources, the OH flux was observed to vary in the same direction as the infrared flux, a fact which strengthens the identification. Unfortunately, OH data on OH 21.5+0.5 are available only near the time of one infrared measurement. Because of the position discrepancy between the radio and infrared sources and because no data on correlated variations exist for OH 21.5+0.5, the identification of this source must be regarded as tentative. We will assume that the infrared and radio sources are associated, for the purposes of this paper. Except for OH 21.5+0.5, we regard the identification of the infrared sources with the OH masers as very secure.

The Palomar Sky Survey red plates were examined for optical candidates. Two sources, OH 30.1−0.2 and OH 45.5+0.1, have optical objects at the level of 20–21 mag within 3″–4″. Finally, infrared and radio positions for OH 26.5+0.6 show that it can be identified with the source known as CRL 2205. This source has also been studied by Low et al. (1976) and by Pipher and Soifer (1976), who obtained high-resolution measurements of the 10 μm feature. OH 45.5+0.1 should not be confused with the 1665 MHz maser of the same name. The 1612 MHz maser studied here is clearly distinct in position from both the 1665 MHz

TABLE 2
Photometry of New Sources*

Source (1)	10.1 μm (Jy) (2)	2.2 μm (Jy) (3)	3.4 μm (Jy) (4)	4.8 μm (Jy) (5)	8.7 μm (Jy) (6)	9.5 μm (Jy) (7)	11.2 μm (Jy) (8)	12.5 μm (Jy) (9)	20 μm (Jy) (10)	Date (11)
OH 21.5+0.5	16 (2)	⋯	0.6 (0.1)	11 (1)	16 (2)	4.3 (0.7)	7.8 (1)	38 (5)	40 (10)	1975 July
	10 (1)	<0.003	0.41 (0.06)	3.5 (0.4)	8 (1)	2.8 (0.3)	3.0 (0.4)	21 (2)	27 (5)	1976 May
OH 26.5+0.6	270 (30)	0.18 (0.05)	32 (3)	160 (20)	240 (30)	82 (15)	160 (30)	490 (90)	660 (200)	1974 July
	200 (20)	⋯	⋯	⋯	220 (30)	70 (10)	130 (20)	410 (60)	300 (90)	1974 Sept.–Oct.
	170 (10)	⋯	20 (2)	130 (20)	170 (20)	47 (5)	102 (10)	370 (40)	400 (100)	1975 June, July, Aug.
	320 (30)	⋯	52 (5)	210 (20)	360 (30)	150 (15)	180 (20)	570 (60)	720 (100)	1976 May
OH 30.1−0.2	24 (2)	0.21 (0.01)	8.6 (0.5)	18 (4)	27 (4)	20 (4)	27 (4)	29 (5)	40 (15)	1974 Sept.–Oct.
	57 (11)	0.70 (0.06)	23 (4)	43 (8)	57 (12)	43 (8)	55 (11)	60 (12)	75 (15)	1975 June–July
	42 (5)	2.8 (0.6)	16 (1)	26 (2)	46 (5)	33 (4)	43 (5)	46 (5)	66 (15)	1976 May
OH 30.1−0.7	60 (7)	2.2 (0.1)	1.0 (0.2)	15 (3)	64 (12)	20 (4)	37 (5)	120 (20)	100 (30)	1974 July
	42 (5)	<0.008	0.72 (0.07)	13 (6)	40 (8)	12 (2)	22 (4)	80 (10)	100 (30)	1975 July, Aug.
	35 (3)	<0.003	⋯	7.2 (0.7)	42 (4)	17 (2)	15 (2)	62 (7)	80 (15)	1976 May
OH 32.8−0.3	10 (1)	⋯	⋯	⋯	11 (2)	2	2.6 (0.5)	19 (4)	⋯	1974 Sept.
	46 (5)	<0.2	1.9 (0.2)	31 (3)	50 (10)	15 (3)	23 (4)	100 (20)	100 (50)	1975 July
	68 (7)	<0.004	6.4 (0.4)	47	84 (9)	34 (4)	28 (3)	110 (10)	200 (50)	1976 May
OH 45.5+0.1	21 (3)	⋯	⋯	⋯	⋯	⋯	⋯	⋯	20 (6)	1974 July
	18 (2)	0.8 (0.1)	5 (1)	10 (2)	15 (2)	13 (2)	17 (2)	15 (2)	⋯	1974 Sept.–Oct.
	10 (2)	0.24 (0.05)	2.7 (0.5)	6 (1)	10 (1)	6.8 (1)	9 (1)	12 (2)	⋯	1975 July
	17 (2)	0.64 (0.06)	6.5 (0.06)	14 (2)	18 (4)	13 (3)	17 (3)	18 (4)	40 (20)	1975 Aug.
	30 (3)	1.8 (0.1)	11 (1)	15 (1)	29 (3)	25 (3)	28 (3)	27 (3)	38 (8)	1976 May

* Numbers in parentheses represent 1 σ errors.

TABLE 3

Derived Properties

Source (1)	OH Velocities (km s^{-1}) (2)	Near Kinematic Distance (kpc) (3)	Far Kinematic Distance (kpc) (4)	[3.4 μm] − [12.5 μm] (mag) (5)	T_c (K) (6)	$\tau_{\rm sil}$ (7)	$L_{\rm near}$ ($10^3 L_\odot$) (8)	$L_{\rm far}$ ($10^4 L_\odot$) (9)	Date (10)
OH 21.5+0.5...	98, 134	7.5	10.9	7.2 (.2)	383 (10)	2.1	16	3.3	1975
				6.9 (.2)	393 (8)	1.8	8	1.6	1976
OH 26.5+0.6...	14, 42	1.8	16.1	5.6 (.2)	464 (16)	1.7	15	120	1974
				5.8 (.2)	452 (10)	1.9	10	79	1975
				5.3 (.2)	489 (10)	1.3	19	150	1976
OH 30.1−0.2...	34, 69	3.1	14.0	4.0 (.2)	601 (20)	0.3	5	9	1974
				3.7 (.3)	633 (34)	0.3	11	22	1975
				3.8 (.1)	621 (15)	0.3	8	15	1976
OH 30.1−0.7...	79, 119	5.5	10.4	...	...	1.6	22	8	1974
				7.4 (.3)	371 (10)	1.7	18	6	1975
				7.5 (.2)	368 (6)	1.1	14	5	1976
OH 32.8−0.3...	46, 77	3.9	12.7	7.0 (.2)	392 (11)	1.8	12	13	1975
				5.8 (.1)	457 (7)	1.2	18	20	1976
OH 45.5+0.1...	18, 53	2.1	11.7	3.9 (.3)	616 (28)	...	1.2	3.7	1974
				4.3 (.3)	571 (25)	0.4	0.6	1.8	1975 July
				3.8 (.3)	625 (28)	...	1.6	4.8	1975 August
				3.6 (.2)	641 (19)	...	2.2	6.8	1976

NOTES.—$\tau_{\rm sil}$ was calculated from the relation:

$$\Delta S_\nu = S_\nu(\text{cont}) \times [1 - \exp(-\tau_{\rm sil})] ,$$

where S_ν(cont) is the continuum flux at 9.5 μm predicted from the T_c in column (6) and ΔS_ν is the difference between the observed and predicted 9.5 μm fluxes (i.e., the depth of the absorption feature). Use of this relation amounts to assuming that the background emission is a blackbody and that the absorption occurs in a uniform, cold layer that produces no emission itself. This technique, compared with more elaborate techniques (cf. Gillett *et al.* 1975), will tend to underestimate $\tau_{\rm sil}$.

masers in this region (see Goss *et al.* 1973), but it does lie near the outer boundary of one of the H II regions in this area (Wynn-Williams, Downes, and Wilson 1971).

b) Photometry and Energy Distribution

The fluxes of the infrared sources found in this study are presented in Table 2. The large uncertainties in the 20 μm flux are due primarily to calibration uncertainties. Because the sources have varied, Table 2 includes separate entries for measurements made at different times. The apparent rapid variation of OH 45.5+0.1 from 1975 July to August is unusual. In no other case did a statistically significant variation occur in such a short period; and some entries in Table 2 represent an average of data obtained over a period of several months, as indicated by the range of dates given in column (11).

The energy distributions between 2 and 20 μm are presented for each of the sources in Figure 1. For comparison, Figure 1 also includes the energy distributions of IRC +10011, the reddest OH maser studied by Hyland *et al.* (1972), and of VX Sgr. The extreme redness of the objects reported here readily explains their absence from the 2.2 μm sky survey and emphasizes the value of searches at long wavelengths. All these sources have energy distributions which peak at much longer wavelengths than previously studied OH/IR objects. The 10 μm feature appears in absorption in at least the four reddest of these sources, while it is characteristically in emission in the sources studied by Hyland *et al.* (1972). Figure 1 also shows energy

distributions at different times to illustrate the nature of the variation. The apparent changes in the 10 μm absorption feature between 1975 and 1976 are due to the use of different filters in 1976. The 1976 filters are centered 0.1–0.2 μm lower in λ than the 1975 filters; this change causes the 11.2 μm point to be lower and the 9.5 μm point to be higher when a 10 μm absorption feature is observed.

c) Color Index and Color Temperature

The 3.4 to 12.5 μm color indices for the sources are given in column (5) of Table 3. The choice of wavelengths for the color index was based on the following considerations. Three of the sources were too weak to be detected at 2.2 μm; thus 3.4 μm was the shortest wavelength where a significant number of data are available. The 12.5 μm point was chosen for the long wavelength value to avoid confusion by the absorption feature at 9.5 μm and because measurements at this wavelength are generally more accurate than at 20 μm.

Color temperatures, T_c, were computed from the [3.4 μm] − [12.5 μm] color index and are presented in column (6) of Table 3. For most of these sources, these temperatures fit the observed points reasonably well only from 3.4 to 12.5 μm, and only if the silicate feature is ignored. The dashed line in Figure 1*b* illustrates the case for OH 26.5+0.6; the observed 20 μm flux is about twice the value predicted from T_c and the 2.2 μm flux is 8 times less than the predicted flux. The two objects with $T_c > 500$ K have properties somewhat different from those of the four objects with $T_c < 500$ K, as will be discussed below. The dashed
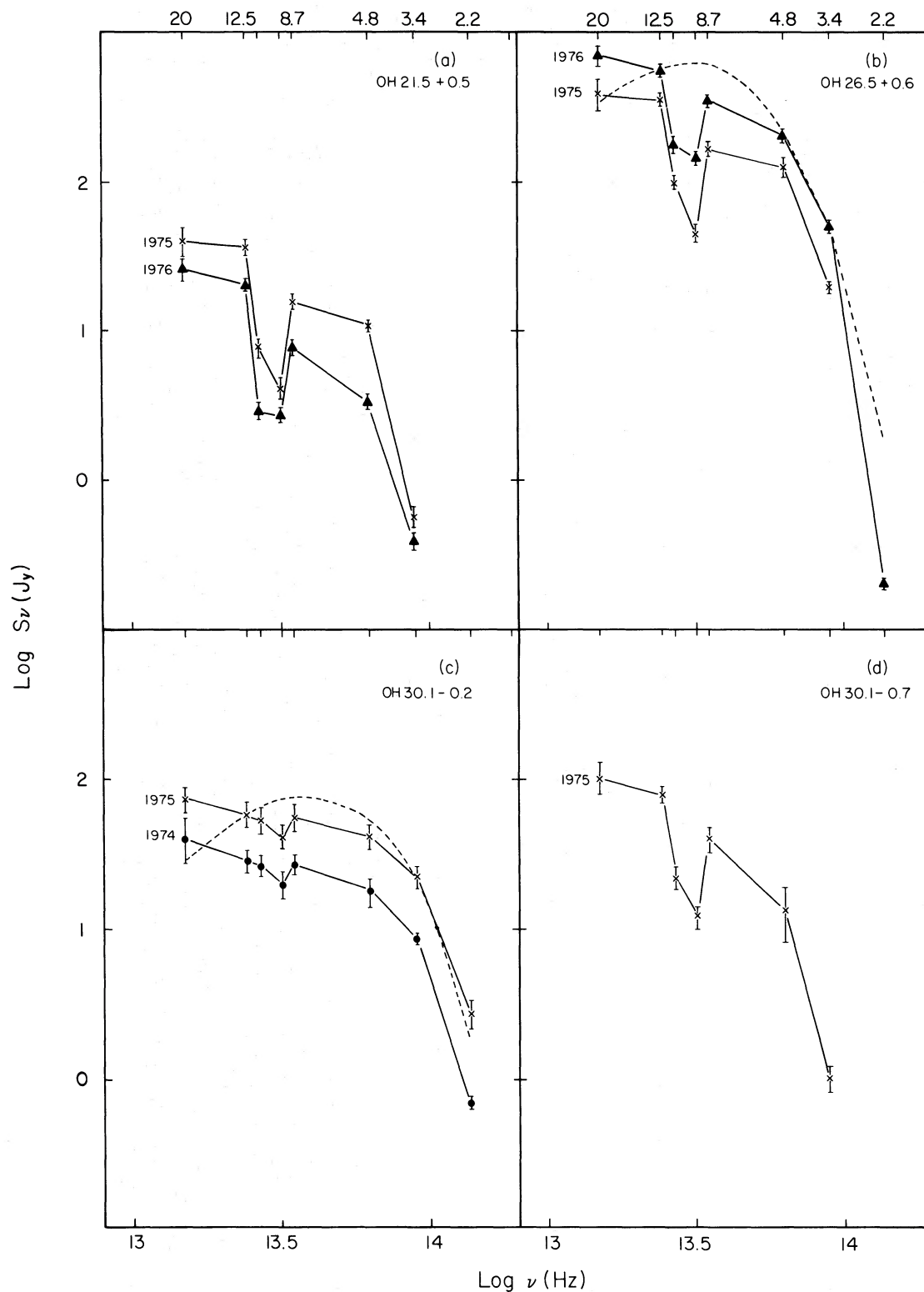
FIG. 1.—The infrared energy distributions of the new sources (a)–(f) and of two previously studied sources (g). The dashed lines in Figs. 1b and 1c are blackbody curves for the color temperature derived from the 12.5 and 3.4 μm measurements. Numbers at the top of the plots represent wavelength in microns.
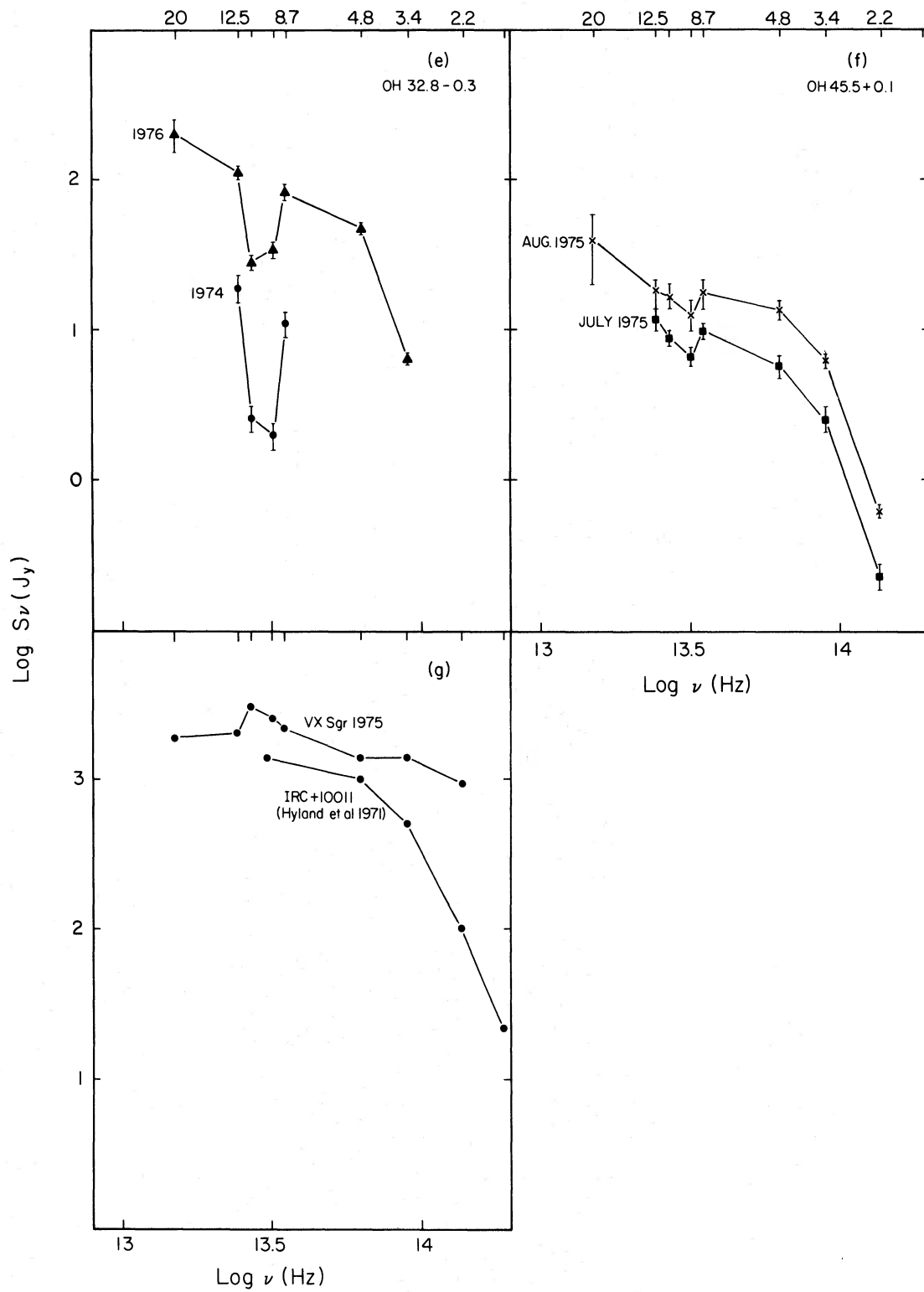
FIG. 1.—*Continued*

line in Figure 1c represents a blackbody at T_c for the case of OH 30.1−0.2. It does appear that none of the sources is radiating as a simple gray body. Variations in T_c which are statistically significant have occurred in OH 26.5+0.6 and OH 32.8−0.3. The sense of the variation is that T_c increases when the luminosity increases.

d) The 10 μm Absorption Feature

The 10 μm absorption feature, presumably due to silicate absorption, is present in at least four of the sources. The optical depth in the feature (τ_{sil}) is given in column (7) of Table 3. None of the secular changes in τ_{sil} are significant. When sources are compared, the optical depth in the silicate feature shows a rough correlation to T_c^{-1}; the absorption is strong in the four sources with $T_c < 500$ K, weak or absent in the two sources with $T_c > 500$ K, and generally absent or in emission in the sources studied by Hyland et al. (1972). It has been suggested (Pipher and Soifer 1976) that, in sources with silicate absorption, substantial corrections to the luminosity are required because of absorption from 10 to 20 μm. In this paper the assumption has been made that the observed luminosity from 2 to 20 μm represents most of the energy radiated by these objects.

e) The 2.3 μm CO Band

Observations of the CO band at 2.3 μm are presented in Figures 2 and 3. For comparison, similar data for 106 Her, an M0 giant, are shown in Figure 2, and data for 30g Her (M1 III) and δ Oph (M6 III) are shown in Figure 3b. It is clear that absorption is
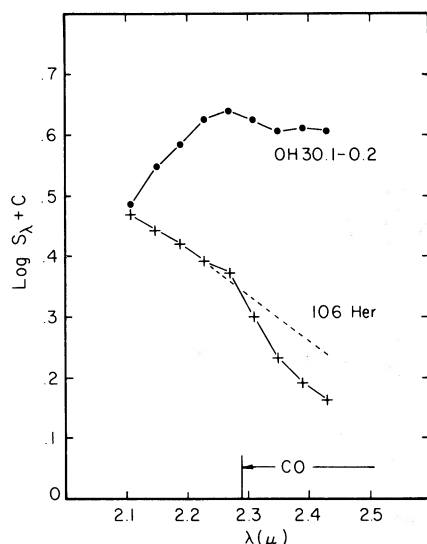
FIG. 2.—Spectra of OH 30.1−0.2 and, for comparison, 106 Her, an M0 giant. These spectra, taken at the Mount Wilson 1.5 m telescope, are an average of data obtained on 1975 September 30 and October 1. S_λ, the flux density per unit wavelength, is used here, as distinct from Fig. 1, where S_ν is used. The dashed line represents a Rayleigh-Jeans approximation to a blackbody spectrum.

present at $\lambda > 2.3$ μm in the spectra of OH 30.1−0.2 and OH 45.5+0.1. On the other hand, OH 26.5+0.6 shows no absorption. If a significant fraction of the observed 2 μm flux comes from radiation by dust surrounding the object, the lack of CO feature in the 2 μm spectrum of OH 26.5+0.6 is to be expected.

IV. DISCUSSION

The discovery of infrared sources near each of the OH masers in the sample is consistent with the association of such masers with infrared sources. Together with evidence of Harvey et al. (1974) that infrared pumping is the cause of the population inversion of the OH, our data support the hypothesis that every double-peaked OH maser which emits principally at 1612 MHz is associated with an infrared object. In § IVa, two infrared pumping models will be discussed in relation to the observations of the sources reported here. Following that discussion, various parameters of the sources will be derived from the observations and used to decide between different possible explanations of the observed energy distributions. The data support the interpretation that the observed radiation originates in a thick circumstellar dust shell. Because of this and because previously studied OH/IR objects were found to have a large range of dust shell thickness (Hyland et al. 1972), we feel that the objects reported here are stars surrounded by dust, but with thicker dust shells. The nature of the object inside the dust shell and its evolutionary state will be discussed briefly, and suggestions for future observations will be made.

a) Pumping of the OH Masers

The observations of correlated variations in OH and infrared flux (Harvey et al. 1974) firmly established radiative pumping for a number of OH masers associated with Mira variables. Although our observations of variation are much less complete, the change of OH flux is always in the same direction as the change of infrared flux, again suggesting a radiative pump.

To determine whether infrared pumping is feasible for the sources reported here, we wish to compare the number of OH photons emitted per second, $n(\text{OH})$, to the number of infrared photons absorbed per second in the transition which pumps the OH molecules, $n(\text{IR})$. The pump efficiency, $\epsilon = n(\text{OH})/n(\text{IR})$, must be less than 1 for infrared pumping, because at least one pump photon is required for each maser photon. The efficiency is related to the observed peak fluxes of OH and infrared energy, $S_\nu(\text{OH})$ and $S_\nu(\text{IR})$, by the following relation:

$$\epsilon = \frac{S_\nu(\text{OH})}{S_\nu(\text{IR})} A_{\text{IR}} \frac{\Omega_{\text{OH}}}{\Omega_{\text{IR}}} \frac{\delta v_{\text{OH}}}{\delta v_{\text{IR}}}, \qquad (1)$$

where Ω is the solid angle into which the observed flux is emitted and δv is the bandwidth in km s⁻¹ for microwave emission or infrared absorption by OH molecules. A_{IR} is the attenuation ($e^{-\tau_{\text{IR}}}$) between the observer and the masing region. In the simplest case, the last
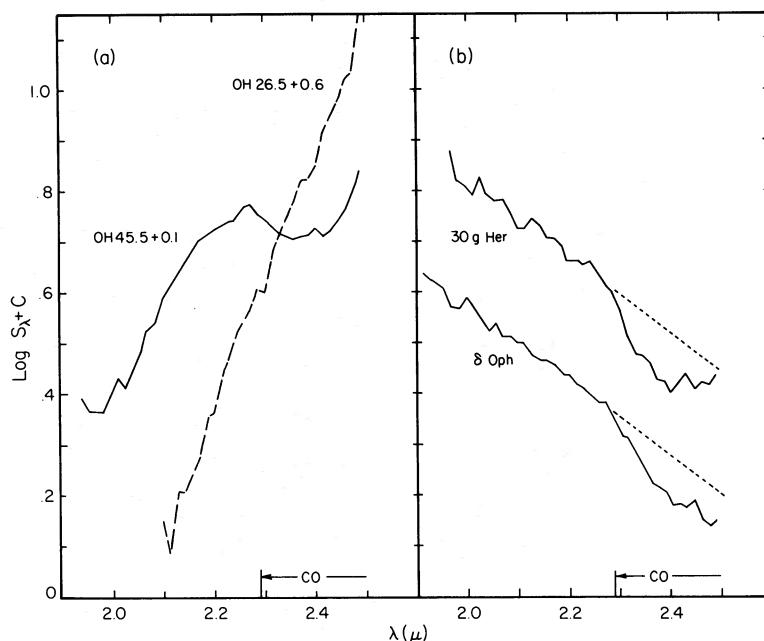
FIG. 3.—Fig. 3a presents spectra of OH 45.5+0.1 and OH 26.5+0.6 (broken line), and Fig. 3b presents spectra of 30g Her (M1 III) and δ Oph (M6 III). These data were obtained on the 2.1 m telescope at Kitt Peak in 1976 June. The raw data were divided by the spectrum of a standard star obtained at similar air mass to remove the effects of atmospheric absorption. The dashed lines in Fig. 3b are the Rayleigh-Jeans approximation to a blackbody spectrum.

two ratios in equation (1) and A_{IR} are equal to 1, and the efficiency is given by the ratio of fluxes.

The two pumps which have been proposed operate at 2.8 and 35 μm (Litvak 1969; Litvak and Dickinson 1972; Elitzur, Goldreich, and Scoville 1976). Neither of these wavelengths is directly accessible to ground-based observations, but interpolation between 2.2 and 3.4 μm provides a reasonable estimate of the 2.8 μm flux. In practice, T_c was used to predict a 2.8 μm flux. Since the 2.2 μm flux, when measured, is always less for the sources than that predicted by T_c, this method should provide an upper limit to the true 2.8 μm flux. Extrapolation of the energy distributions in Figure 1 to 35 μm is more uncertain, especially because of the large calibration uncertainties at 20 μm. We have taken the flux at 35 μm equal to the 12.5 μm flux for the purpose of discussing pumping models. This probably represents a lower limit to the 35 μm flux. We have not used T_c to predict the 35 μm flux because all the sources indicate an excess at 20 μm over that predicted by T_c. The OH fluxes are given in column (2) of Table 4, and the flux ratios for 12.5 and 2.8 μm are given in columns (3) and (4) of Table 4. The ratios in column (4) cannot be reconciled with pumping at 2.8 μm unless the correction factors involving solid angle, bandwidth, or attenuation are much less than 1.

While Ω_{IR} is certainly equal to 4 π, the solid angle of emission for the OH may be less than 4 π for any given source. Highly directional maser emission would be hard to reconcile with the high percentage of OH masers observed among the reddest oxygen-rich Mira variables (Hyland et al. 1972), but the presence of inhomogeneities in the shell that give rise to maser

emission which varies with direction is certainly plausible. However, it is unlikely that all these sources emit most intensely in our direction, unless the sample is biased in favor of strong sources. Thus the possibility that $\Omega_{OH} < 4 \pi$ cannot be ruled out, but on the average a very small value of Ω_{OH}/Ω_{IR} is unlikely.

The ratio $\delta v_{OH}/\delta v_{IR}$ will equal 1 if the infrared radiation is produced far inside the region where the maser emission originates, because the radial-velocity dispersion in the shell will determine both the absorption, and emission-line widths for the OH molecules. If, on the other hand, the infrared radiation is produced in an expanding circumstellar shell, geometrical effects

TABLE 4

COMPARISON OF OH AND INFRARED FLUXES

Source (1)	$S_v(OH)$* (2)	$\dfrac{S_v(OH)\dagger}{S_v(12.5\ \mu m)}$ (3)	$\dfrac{S_v(OH)\dagger}{S_v(2.8\ \mu m)}$ (4)	$\dfrac{2\delta v_{OH}}{\Delta V}$ (5)
OH 21.5+0.5...	22	0.58	220	1/12
OH 26.5+0.6...	170	0.46	35	1/20
OH 30.1−0.2...	14.2	0.24	1.4	1/13
OH 30.1−0.7...	47	0.59	310	1/14
OH 32.8−0.3...	21	0.21	62	1/4
OH 45.5+0.1...	4.5	0.38	4.5	1/13

* These fluxes are from OH measurements made in 1975 June. The average of the peak fluxes in the two OH velocity peaks was used for $S_v(OH)$.

† These flux ratios are derived from the OH observations (col. [2]) from 1975 June and the infrared observations (Table 1) of 1975 June–July. The 2.8 μm fluxes were calculated from T_c (Table 2).

may make $\delta v_{IR} > \delta v_{OH}$ (Elitzur, Goldreich, and Scoville 1976). In the model suggested by those authors, the two OH velocity peaks are produced in the near and far sides of an expanding circumstellar shell at a radius $\sim 10^{16}$ cm. In this model, $\delta v_{IR} \leq \Delta V/2$, where ΔV is the velocity separation of the two peaks; thus $\delta v_{OH}/\delta v_{IR} \geq 2\delta v_{OH}/\Delta V$, given in column (5) of Table 4. While this factor would make 2.8 μm pumping plausible for two of the sources, it fails for the other four. Furthermore, in the model of Elitzur *et al.*, most of the 35 μm photons and essentially all the 2.8 μm photons would be produced from well inside the maser region. The results of § IV*e* indicate a dust shell radius of 10^{15} cm, consistent with these predictions. For 2.8 μm photons, the ratio $\delta v_{OH}/\delta v_{IR}$ is almost certainly ~ 1 in this model.

The probability that A_{IR} is substantially less than unity at 2.8 μm is difficult to assess generally. In the model of Elitzur *et al.* the maser region is on the outer edge of the expanding shell, and little or no attenuation would exist between the maser region and the observer. This picture is supported by VLBI measurements of the OH maser emission (Reid 1975), combined with occultation data on the infrared emission.

While 2.8 μm pumping cannot be strictly ruled out, it must be considered extremely unlikely for these sources. In contrast, 35 μm pumping appears feasible on the basis of the efficiencies in column (3) of Table 4. Although the statistics are poor, the fact that the efficiencies in column (3) are confined to a range from 0.21 to 0.59 also supports 35 μm pumping, since that model would predict a linear relationship between the two fluxes. In contrast, the efficiencies for 2.8 μm pumping range from 1.4 to 310, indicating that a plot of the OH flux versus the 2.8 μm flux would produce a scatter diagram. The conclusion that 35 μm pumping is far more likely than 2.8 μm pumping for the sources in this sample cannot immediately be extended to apply to previously studied objects; as will be discussed, the relationship of these sources to other OH/IR objects is not clear. It should be noted that the above discussion of pumping models depends only on the observed OH and infrared fluxes and is therefore independent of the following discussion of source properties.

b) Distance

The kinematic distances to the objects, derived from a Schmidt model of galactic rotation, are given in Table 3. Because all the sources lie at low galactic longitudes, both a near kinematic distance (column [3]) and a far kinematic distance (column [4]) are possible. Besides this usual ambiguity, additional uncertainty is caused because the velocity of the infrared source relative to the two OH velocity peaks is not known. Rather than trying to evaluate various models for the geometry of the objects, we have assumed a source velocity midway between the two OH peaks (column [2]). The uncertainty in the stellar velocity generally results in an uncertainty for the distance of 1 kpc.

The validity of kinematic distances to these objects is certainly open to question, especially since most previously studied OH/IR objects were Mira variables, for which kinematic distances are generally not meaningful. However, the longest-period Mira variables have a galactic distribution and kinematic properties consistent with Population I objects (Smak 1966). Furthermore, studies of the galactic distribution of the unidentified OH sources indicate that differential rotation must be a significant component of the motion of many of these sources, suggesting that these are also Population I objects (Caswell 1974; Bowers 1975). Further evidence that many of these sources are Population I objects is the pronounced clustering at longitudes near the tangential points of major spiral arms, where other Population I objects, like H II regions, are seen to cluster (Bowers 1975). Caution must be exercised in using kinematic distances for any particular source. There are examples of sources with noncircular velocities, and Bowers (1975) suggests a mixture of Population I objects and Population II objects.

c) Luminosity

The luminosities of the objects were calculated by assuming the kinematic distance and integrating the observed energy distributions from 2 to 20 μm. It is assumed that this represents the true luminosity of each object, with most of the error coming from poor distance information. The luminosities which result from assuming the near kinematic distance (column [8] of Table 3) cluster around $10^4 L_\odot$, except for OH 45.5+0.1, which is closer to $10^3 L_\odot$. The internal agreement of the luminosities supports the use of the near kinematic distance in the majority of cases. Use of the far kinematic distances (column [9] of Table 3) results in a significantly larger scatter in the derived luminosities. Averaging over all measurements of all sources should yield a rough average over period; the result from all 17 measurements is $\langle L \rangle \approx (1.1 \pm 0.7) \times 10^4 L_\odot$, using the near kinematic distance. If the far kinematic distance is used, the mean result is $2.8 \times 10^5 L_\odot$, but the rms scatter of all the values is $4.5 \times 10^5 L_\odot$. The stated errors in these quantities do not reflect possible systematic errors. Since contributions from $\lambda > 20$ μm are neglected and no corrections for attenuation are included, the true $\langle L \rangle$ may well be larger. If the near kinematic distances are used to compute luminosities, the sources appear to be comparable with the most luminous of known Mira variables (cf. Smak 1966). If the far kinematic distances are used, some of the sources have a luminosity comparable with that of the supergiants VY CMa and VX Sgr, two of the previously studied OH/IR stars, but OH 26.5+0.6 would have a luminosity of $\sim 10^6 L_\odot$.

d) Extinction

The silicate absorption feature in four of the sources is evidence that a substantial amount of cold material lies between the observer and the object emitting at 10 μm. Viewed most generally, there are three possible

TABLE 5

Molecular Line Observations

Source (1)	T_A^*(CO) (K) (2)	V† (km s^{-1}) (3)	ΔV (km s^{-1}) (4)	T_A^*(^{13}CO) (K) (5)	V (km s^{-1}) (6)	ΔV (km s^{-1}) (7)
OH 21.5+0.5.......	< 2	60 to 160	...	< 0.8	...	...
OH 26.5+0.5.......	< 1	−20 to +70	...	< 0.8	...	...
OH 30.1−0.2.......	< 3	0 to 100	...	1.0	105	3
OH 30.1−0.7.......	3	80	~10	1.2	86	1
OH 32.8−0.3.......	2	90	...	1.5	91	1
	3	80	...	1.0	81	3
OH 45.5+0.1.......	8	58	~10	1.3	58	6

† When no line was detected, the velocity range covered is given.

explanations of this extinction: general interstellar extinction; localized extinction caused by molecular clouds associated with the object; or very local extinction caused by a thick dust shell surrounding the object.

If the extinction were due to general interstellar extinction, correlations would be expected between the distance and τ_{sil}, as well as between the distance and the [3.4 μm] − [12.5 μm] color index. Examination of Table 3 indicates that these correlations are not present. Furthermore, the extinction to four of the objects is very large; to make the color index equal to that of IRC +10011, the reddest of previously known OH/IR stars, 2–4 mag of extinction at 3.4 μm are required if no extinction at 12.5 μm is assumed. For comparison, there are 1.2 mag of extinction at 3.4 μm to the galactic center (Becklin and Neugebauer 1968). Although it is possible that all six of these objects lie in directions of extremely high interstellar extinction, we consider it to be very unlikely.

The 3.4 μm extinctions inferred above would imply extinction at visible wavelengths (A_v) of 45–90 mag, an extinction which is inferred in some massive molecular clouds. Observations of the $J = 1 \to 0$ transition of ^{12}CO show that no strong sources of molecular emission exist in the direction of any of these objects, as seen in Table 5. Furthermore, ^{13}CO observations indicate that no molecular cloud with $A_v > 10$ mag exists in the direction of these sources within a velocity range of 174 km s^{-1} centered on the mean OH emission velocity.

It is attractive to suppose that the extinction is very local to each object, because: (a) the observed distribution of energy would arise naturally from radiation by warm dust; (b) previous studies of OH/IR sources have interpreted the infrared emission at λ > 3 μm as arising from warm, circumstellar dust; and (c) circumstellar dust shells would be expected if these objects are similar to previous objects which were late-type stars undergoing mass loss. We believe that the infrared emission arises in a warm dust shell surrounding an object, possibly a very late-type star, which is undergoing mass loss. In addition to the mentioned reasons for taking this point of view, the model of OH emission presented by Elitzur, Goldreich, and Scoville (1976) follows naturally from our interpreta-

tion. In § IVe, a very oversimplified model is presented to support this interpretation.

e) Dust Shells

The model consists of a late-type star of luminosity ~ 10^4 $L_\odot$ surrounded by a thick circumstellar dust shell. The color temperatures in Table 2 suggest mean dust temperatures around 500 K. The existence of the silicate absorption feature and the 20 μm measurement indicate that a substantial amount of dust at lower temperatures must also exist. If radiation-transport effects are ignored, for a luminosity of 10^4 $L_\odot$ and a constant emissivity from the visible to 10 μm, the dust must lie at a distance of 5 × 10^{14} cm from the star in order to reach 500 K. This diameter agrees with that found by occultation experiments (Zappala et al. 1974) on IRC +10011. If the emissivity is taken to be constant shortward of 1 μm, and to go as λ^{-1} for λ > 1 μm, then the derived distance from the star is 10^{15} cm. These examples indicate that circumstellar dust shells provide a reasonable explanation for the appearance of the energy distributions.

The time variations in T_c are also readily explained in a dust shell model. The equilibrium temperature of dust grains at a given distance from a luminous star is proportional to L^b, where L is the luminosity and $b = 0.20 - 0.25$, depending on the wavelength dependence of the grain opacity. The observed fractional variation of T_c is 0.1−0.4 of the fractional variation of L in the two cases of significant variation. Within the uncertainties of measurement, these data are consistent with theoretical expectations. This interpretation is also consistent with the picture developed by Elitzur, Goldreich, and Scoville (1976). In that picture the variations in the OH flux are caused by changes in the 35 μm flux of pumping photons due to variations in the dust temperature. The variations in dust temperature are in turn driven by luminosity variations of the central star.

f) Evolutionary State

Two of the objects presented here (OH 30.1−0.2, OH 45.5+0.1) have energy distributions which are reasonably similar to those of previously studied OH/IR stars, but the other four objects have energy

distributions which are nearly identical to those found in objects embedded in molecular clouds. It is not possible to rule out a pre–main-sequence object as the explanation of any of these sources, but there is considerable evidence against that explanation. The double-peaked OH velocity profile, the time variability, and the absence of strong molecular radio emission are all characteristics which distinguish these objects from known pre–main-sequence objects. For OH 30.1−0.2 and OH 45.5+0.1, the detection of absorption in the 2.3 μm CO band is further evidence in favor of a late spectral type.

g) Comparison with Other OH/IR Objects

The majority of previously studied OH/IR objects were Mira variables. The galactic distribution of the unidentified OH objects suggested that many are Population I objects, unlike most Mira variables but like those with the longest periods. The nondetection of absorption in the 2.3 μm CO band in OH 26.5+0.6 may appear to argue against a late spectral type, but the feature could well be obscured by overlying dust emission, since the dust shell around OH 26.5+0.6 must be considerably thicker than those around any of the previously studied OH/IR objects.

A strong relation between stellar period and separation of the two OH velocity peaks exists for previously known OH/IR stars (Dickinson and Chaisson 1973; Dickinson, Kollberg, and Yngvesson 1975). The relation given by Dickinson et al. was used to derive periods for the objects reported here from their velocity separations. These derived periods range from 600 to 770 days. Harvey et al. (1974) noted that a positive correlation existed between the [3.5 μm] − [10.1 μm] color and the period of the stars in their sample.

Present infrared data are insufficient to determine the periods of the objects presented here. When the [3.5 μm] − [10.1 μm] color is compared to the derived period based on the velocity separation of the OH peaks, no correlation can be found. Thus it appears that at least one of the correlations noted in other OH/IR stars is absent in these sources.

Elitzur, Goldreich, and Scoville (1976) have argued that the large mass-loss rates (3×10^{-5} $M_\odot$ yr^{-1}) of OH/IR stars like IRC +10011 indicate that they are precursors of planetary nebulae. Because four of the objects reported here have much thicker dust shells than IRC +10011, they probably have a higher mass-loss rate. In this case, they could represent a further evolution toward formation of planetary nebulae.

h) Suggestions for Future Observations

The objects presented in this study have energy distributions with extremely cool ($\sim$500 K) color temperatures. It is likely that all of the observed energy results from radiation by dust at temperatures around 500 K. Because these objects are relatively isolated from molecular clouds and H II regions and because the objects vary in luminosity by large amounts, it may be possible to learn some of the properties of the dust through further observations of these objects.

The variation of the luminosity (L) allows one to measure the variation in other quantities (e.g., the color temperature, T_c) which should vary with the luminosity. Other variables, such as the size and density distribution in the dust shell and the grain composition, would not change appreciably on the time scale of a luminosity variation. In a simple isothermal model where radiative transport is neglected, $T_c \approx L^b$, where $b = 0.20$ for a λ^{-1} opacity law and $b = 0.25$ for a λ^0 opacity law. While a more realistic model of the transport would change the details, different opacity laws should still predict different fractional variations in T_c in response to a given luminosity variation. While the observations of variation in T_c presented here are not accurate enough to distinguish between opacity laws, future observations during large luminosity variations may be able to decide this question.

Some models of radiative transport have suggested that a correlation of $\tau_{\rm sil}$ and T_c^{-1} should exist (Kwan and Scoville 1976). Comparisons from source to source support this suggestion, as discussed above, but no significant secular variation in $\tau_{\rm sil}$ could be observed. Future observations may test this suggestion.

Finally, these objects may help to settle a controversy over corrections to the total luminosity for sources with deep silicate features. It has been argued that the true luminosity of sources with deep silicate features is substantially larger than the observed luminosity, owing to continuum absorption from 10 to 20 μm (Pipher and Soifer 1976). If this energy is reradiated in the far-infrared, then longer wavelength measurements should determine the total luminosity. Such measurements are difficult to interpret for objects in molecular clouds, where nearby H II regions often confuse matters. Since the OH/IR objects appear to be isolated, far-infrared measurements of them should be relatively easy to interpret.

V. SUMMARY

An infrared source has been found near each of six OH masers which emit principally at 1612 MHz in two distinct velocity ranges, suggesting that every OH maser of that type is associated with an infrared object. All the sources have varied in time, and significant variations in color temperature have been observed in two cases. The 2–20 μm energy distributions of the six objects fall into two categories. Two of the distributions are similar to those of the reddest OH/IR objects that had been studied previously. Absorption in the 2.3 μm band of CO has also been detected in these two sources; similar absorption was observed in previously studied OH/IR objects and is indicative of a late spectral type. The remaining four sources have much redder energy distributions and show substantial silicate absorption features.

The energy distributions of these sources indicate that pumping by 35 μm photons is feasible, but that 2.8 μm pumping is very unlikely. This conclusion does not depend on the less direct discussion of the distance,

luminosity, and ultimate nature of the sources which follows.

If the near kinematic distances are used, the sources have luminosities $\sim 10^4 L_\odot$, similar to that of previously studied OH/IR objects. The energy distributions are best explained as emission from very thick dust shells at temperatures of about 500 K. A dust shell model is also consistent with the size of the observed variations in color temperature.

While the nature of the objects inside the dust shell is uncertain, a pre–main-sequence explanation appears unlikely. No sources of strong molecular emission are observed in the direction of these objects, and the time variation distinguishes these objects from known pre–main-sequence objects. Thus they are more likely to be related to M-type Mira variables or M supergiants, which constitute the class of previously studied OH/IR objects. However, present data are insufficient to identify these objects as either Miras or M supergiants. Furthermore, four of the objects in this study do not exhibit some of the relationships between velocity separation, period, and color that were observed for other OH/IR objects. The very thick dust shells suggest an evolution past that of other OH/IR objects, perhaps leading to planetary nebula formation.

REFERENCES

Andersson, C., Johansson, L. E. B., Goss, W. M., Winnberg, A., and Rieu, N.-Q. 1974, *Astr. Ap.*, **30**, 475–477.
Becklin, E. E., and Neugebauer, G. 1968, *Ap. J.*, **151**, 145.
Beckwith, S., Evans, N. J., II, Becklin, E. E., and Neugebauer, G. 1976, *Ap. J.*, **208**, 390.
Bowers, P. F. 1975, *Proc. Astr. Soc. Australia*, **2**, 362.
Caswell, J. L. 1974, in *IAU Symposium No. 60, Galactic Radio Astronomy*, ed. F. J. Kerr and S. C. Simonsen III (Dordrecht: Reidel), p. 423.
Dickinson, D. F., and Chaisson, E. J. 1973, *Ap. J. (Letters)*, **181**, L135.
Dickinson, D. F., Kollberg, E., and Yngvesson, S. 1975, *Ap. J.*, **199**, 131–134.
Elitzur, M., Goldreich, P., and Scoville, N. 1976, *Ap. J.*, **205**, 384–396.
Evans, N. J., II. 1976, private communication.
Evans, N. J., II, Crutcher, R. M., and Wilson, W. J. 1976, *Ap. J.*, **206**, 440.
Gillett, F. C., Forrest, W. J., Merrill, K. M., Capps, R. W., and Soifer, B. T. 1975, *Ap. J.*, **200**, 609.
Goss, W. M., Lockhart, I. A., Fomalont, E. B., and Hardebeck, E. G. 1973, *Ap. J.*, **183**, 843–850.
Harvey, P. M., Bechis, K. B., Wilson, W. J., and Ball, J. A. 1974, *Ap. J. Suppl.*, **27**, 331–358.

Hyland, A. R., Becklin, E. E., Frogel, J. A., and Neugebauer, G. 1972, *Astr. Ap.*, **16**, 204–219.
Kwan, J., and Scoville, N. Z. 1976, *Ap. J.*, **209**, 102.
Litvak, M. M. 1969, *Ap. J.*, **156**, 471.
Litvak, M. M., and Dickinson, D. F. 1972, *Ap. Letters*, **12**, 113.
Low, F. J., Kurtz, R. F., Vrba, F. J., and Rieke, G. H. 1976, *Ap. J. (Letters)*, **206**, L153–L155.
Neugebauer, G., Becklin, E. E., Beckwith, S., Matthews, K., and Wynn-Williams, C. G. 1976, *Ap. J. (Letters)*, **205**, L139.
Neugebauer, G., and Leighton, R. B. 1969, *Two Micron Sky Survey: A Preliminary Catalog* (NASA SP-3047).
Pipher, J. L., and Soifer, B. T. 1976, *Astr. Ap.*, **46**, 153.
Reid, M. J. 1975, Ph.D. thesis, California Institute of Technology.
Smak, J. I. 1966, *Ann. Rev. Astr. Ap.*, **4**, 19.
Wilson, W. J., and Barrett, A. H. 1968, *Science*, **161**, 778.
Winnberg, A., Goss, W. M., Höglund, B., and Johansson, L. E. B. 1973, *Ap. Letters*, **13**, 125–131.
Wynn-Williams, C. G., Downes, D., and Wilson, T. L. 1971, *Ap. Letters*, **9**, 113.
Zappala, R. R., Becklin, E. E., Matthews, K., and Neugebauer, G. 1974, *Ap. J.*, **192**, 109.

N. J. Evans II: Department of Astronomy, University of Texas, Austin, TX   78712

S. Beckwith: Department of Physics, 320-47, California Institute of Technology, Pasadena, CA   91125